

Deep-seated landslide detection with an InSAR time series in the area of Jujuy and Salta, Argentina

Nicolas Garcia Ospina

April 10, 2021

Abstract

Identification and mapping of deep-seated landslides or unstable terrains is a very important topic for the communities to understand, since these are a constant threat, preparation and correct decisions are vital to prevent life and economical loses. For this reason, this kind of maps must be done and constantly revised, even in remote areas. In this report the LiCSBAS package is used to create a InSAR time series in an area in the NW part of Argentina. With this time series a LOS velocity field is produced and later morphed into a downslope velocity model to propose areas with slow moving landslides. In total 251 potential polygons were mapped where the terrain moves at more than 10 mm/year, also 11 zones were found with velocities higher than 25 mm/year. The approach used here has a coarse resolution, but it can cover large areas very fast with low computational demands.

Keywords: Argentina, Downslope, InSAR, landslide, LiCSBAS, velocity

1 Introduction

Deep-seated landslides are a type of gravitational mass movement, whose low but constant speed is imperceptible to the naked eye, still they provide the most amount of sediment over time on river systems as well as big participation in landscape shaping (Swanson & Swanston, 1976; Iverson, 2000). Brueckl *et al.*, 2013, showed an example of how a deep-seated landslide can accelerate due to high precipitations, snowmelt and earthquakes. For this reason the identification and mapping of these landslide comes in handy for further monitoring, thus help authorities make decisions that prevent life and economical losses.

With the continuous growth and availability of Synthetic Aperture Radar (SAR) imagery, its applications have been increasing as well. In the same way, the computational power to process and analyze these large data volumes increases as well. For this reason, the novel LiCSBAS package (Morishita, 2020) was used, this is a lightweight and fast approach to produce InSAR time series and velocity fields.

Within this report the [LiCSBAS](#) package was used to generate a time series from a set of interferograms available for a tile in the Sentinel-1 descending track processed by the

[LiCSAR](#) framework. This time series was then post-processed and analyzed. Interferograms were corrected with the tropospheric delay maps provided by [GACOS](#). The study area is located in the province of Jujuy in the northwestern part of Argentina.

2 Study Area

The study area is located in the NW Argentinian Andes (Figure 1), specifically in the eastern flank, close to the west of the provinces of Jujuy and Salta. The area is composed by a part of the Eastern Cordillera, and the Subandean ranges, which are the intermediate zone between the Puna plateau highlands and the Chaco plain foreland (May, 2008). The area contains many streams (up to fifth order) that feed the Quesera, del Morado, Potrero Castillo and Rosario rivers. This is a vast arid and semi arid area, where the climate in this area is deeply influenced by the South American Summer Monsoon, where 2 seasons are distinguished, a dry season during the austral winter and a rainy season for the austral summer (Bianchi & Yañez, 1992; Garreaud & Aceituno, 2007; Esper *et al.*, 2020).

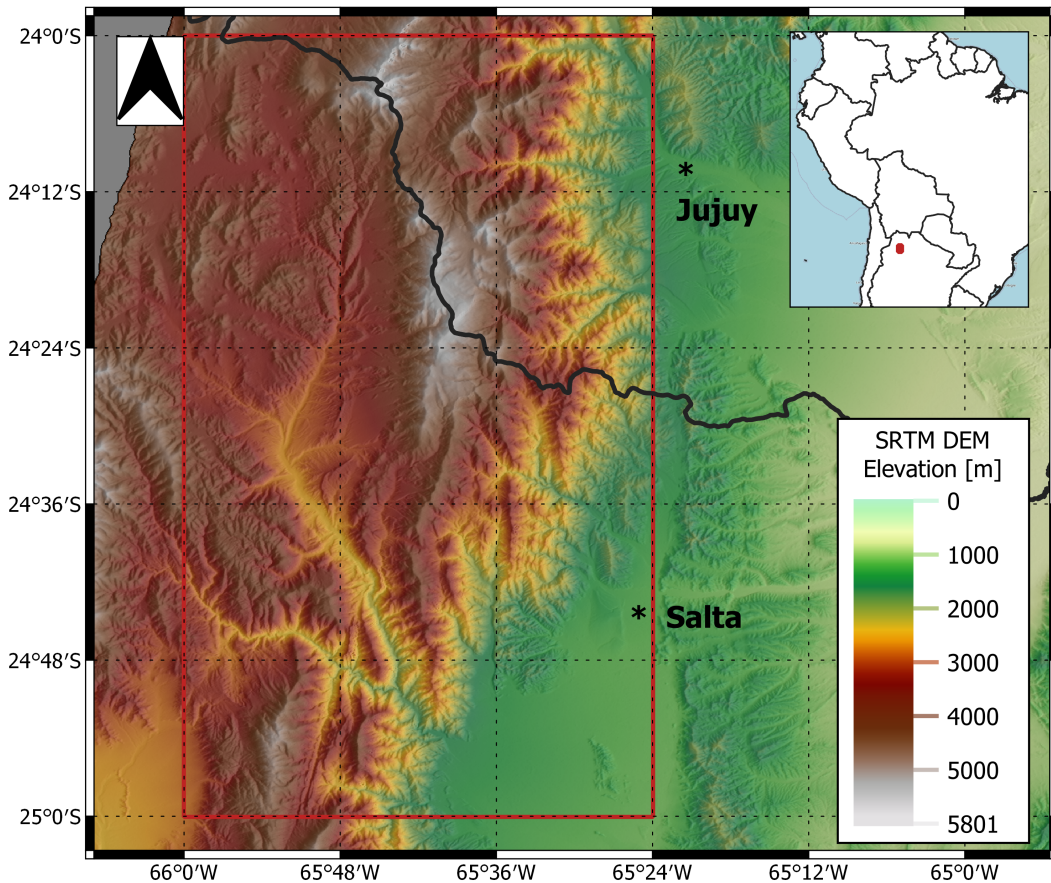


Figure 1: Regional elevation map, the red rectangle represents the study area bounding box.

In a broad sense the geology of the area is composed by a sedimentary-metamorphic Pre-cambrian basement with, greywackes and low grade metamorphic pelites. The basement is

intruded by Cambrian granites and granodiorites. On top of it, there is a complex and discontinuous sedimentary sequence with different continental and marine sedimentary formations dated from Cambrian up to more recent Cenozoic ages (SEGEMAR, 1998; SEGEMAR, 2008), all of these rocks appear to be controlled by N-S direction folds and faults.

3 Data and methods

3.1 Data

In order to capture the surface deformation of a region the method of SAR interferometry (InSAR) can be applied as long as the data acquisition of two SAR images follows a repeat-pass configuration. This means that two radar images are taken with the same instrument at almost the same position, and the only different parameter is the acquisition times (Hanssen, 2001). Radar observations include the returning intensity and phase of a wave front, InSAR makes use of the phase difference between acquisitions and produce interferograms, which can be further translated in displacement relative to the satellite position. This displacement is also known as Line of Sight (LOS) displacement.

A time series of unwrapped interferograms produced by LiCSAR (COMET, 2020) with Sentinel-1 imagery was used. For the selected area the frame 010D_11455_131313 was available. This frame consists of 407 interferograms from 108 acquisitions between August 2014 and January 2021 on the satellite descending track. These interferograms come with their respective coherence maps at a spatial resolution of 0.001° . The temporal resolution of this time series varies between 24 and 12 days, this is because the Sentinel-1B satellite was not operating before 2017 (Morishita, 2021). Finally, it is important to acknowledge the presence of gaps in the time series due to missing acquisitions, the longest one occurs between August 2017 and May 2018.

3.2 LiCSBAS processing

In order to process the set of interferograms, the LiCSBAS v1.5.0 package was used (Morishita *et al.*, 2020). The general LiCSBAS processing chain involves 11 steps where the interferograms are properly stacked. Afterwards, the signal is corrected using the Generic Atmospheric Correction Online Service (GACOS) dataset in order to remove the delay produced by the spatial differences in water vapor content which can sum displacements up to 10-14 cm (Yu *et al.* 2018), low quality pixel removal and then a time series analysis is performed while assessing pixel quality controls, here all the steps were applied. Morishita *et al.*, 2020 lists the LiCSBAS processing steps as follows:

- Step 0–1: Download [LiCSAR](#) products from the official web server
- Step 0–2: Convert GeoTIFF (and Downsample)
- Step 0–3: Tropospheric delay removal using [GACOS](#)
- Step 0–4: Mask interferograms

- Step 0–5: Clip interferograms to the bounding box: (66W, 65.4W, 25.0S, 24.0S)
- Step 1–1: Quality check and identify bad interferograms based on average coherence
- Step 1–2: Loop closure check and identify bad interferograms
- Step 1–3: Small baseline inversion using NSBAS (López-Quiroz *et al.*, 2009; Doin *et al.*, 2011)
- Step 1–4: Calculate standard deviations of the velocity
- Step 1–5: Mask time series with noise indices
- Step 1–6: Spatio-temporal filtering of the time series

3.3 LOS and Downslope velocity field calculation

The resulting output from the LiCSBAS processing is a data cube with cumulative displacement values in millimeters distributed in space and time. LiCSBAS interpolates the data gaps under the assumption that displacement is linear on the long term (Weiss *et al.*, 2020). For the entire study area, the long term deformation trends were calculated by fitting first degree polynomials over each time series using the least squares approximation (Equation 1), which represent the amount of surface displacement per unit of time. These displacement ratios are measured in relation to an almost constant satellite position, for this reason these are here called LOS velocities.

$$E = \sum |p(x_i) - y_i|^2 \quad (1)$$

LOS velocities are vectors directed towards the satellite, and they are a combination of east (E), north (N), and upward (UP) direction movements, these vectors are defined by the flying direction of the satellite and the view angle to the surface, also they are provided as well in the LiCSAR metadata. In order to estimate the surface velocities for deep-seated landslides and unstable terrains, the velocity vectors are projected along the slope vectors which can also be decomposed into north, east and upward components. Cascini *et al.*, 2010, describes how to use the DEM derived gradient (Equation 2) and the aspect in radians (Equation 3) to decompose the slope vector into the E, N and UP components (Equation 4). Using the LOS velocity vectors (V) and the slope vector (S) components, the LOS velocities can be projected to the steepest slope using the scalar projection (Equation 5).

$$\phi = \left(\frac{180}{\pi} \right) * \arctan \sqrt{\left(\frac{dz}{dy} \right)^2 + \left(\frac{dz}{dx} \right)^2} \quad (2)$$

$$\alpha = \left(\frac{180}{\pi} \right) * \arctan 2(dy, -dx) + 180^\circ \quad (3)$$

$$S = \begin{bmatrix} S_E \\ S_N \\ S_{UP} \end{bmatrix} = \begin{bmatrix} -\sin(\alpha)\cos(\phi) \\ -\cos(\alpha)\cos(\phi) \\ \sin(\phi) \end{bmatrix} \quad (4)$$

$$V_S = ||V||\cos\theta = \frac{V \cdot S}{||S||} \quad (5)$$

Finally, the velocity fields were used to quantitatively analyze a single landslide as well as making a regional map of potential unstable terrains where downslope velocities were higher than 10 and 25 mm/year, this zonation was done on a GIS environment. Figure 2 shows the topographic features as well as the slope decomposition for the landslide analyzed. The same data was built for the entire study area.

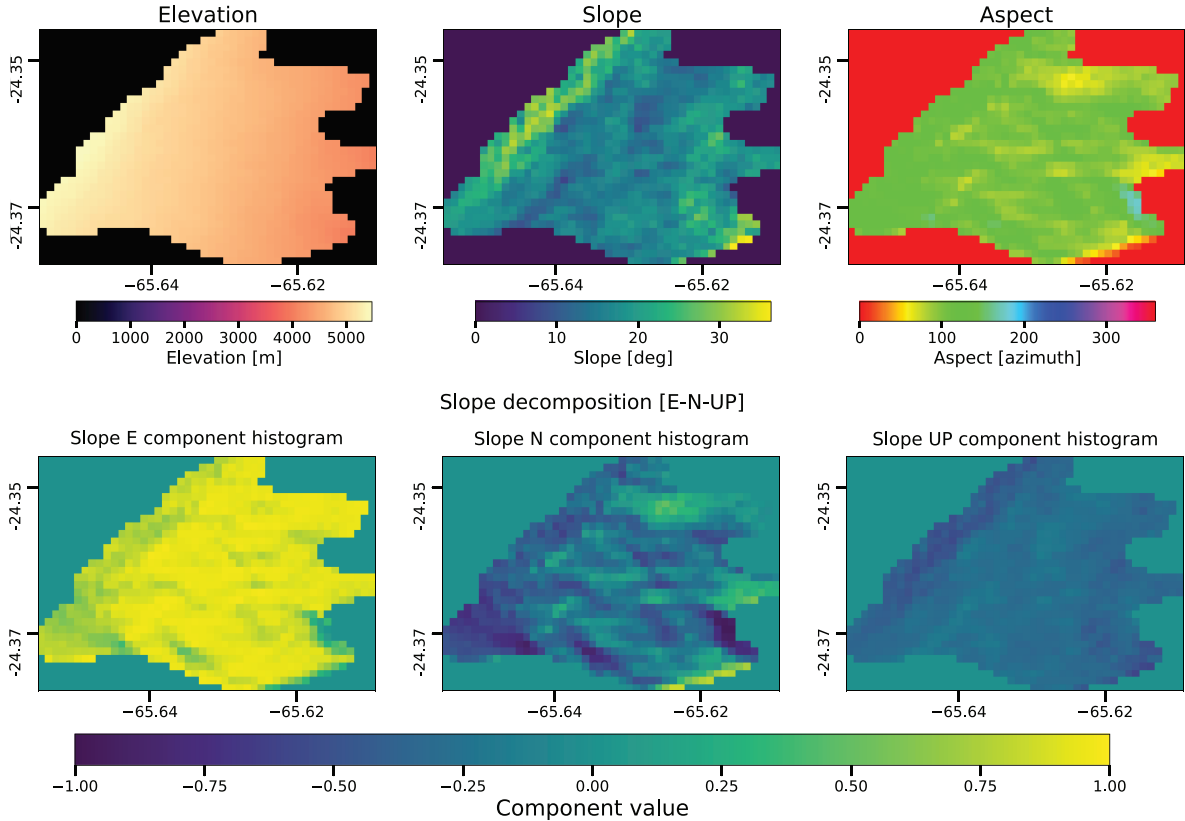


Figure 2: Topographic features and slope East, North and Upwards components

3.4 Seasonal variations detection

Landslides are highly influenced by soil water content and their behavior varies between dry and rainy seasons. Even though, the area is characterized as an arid zone with a low mean annual rainfall, it is worth to use the InSAR time series to broadly assess the seasonal influence in the slow moving landslides. This assessment was done after removing the long term trend with the backwards finite difference method (Equation 6), where for each value x_t starting on the second one, the previous one x_{t-1} is subtracted, therefore the cumulative behavior is diminished. Figure 3 displays the velocity map of the area with a sample time series with the calculated velocity and detrended deformation, these are the base of the velocity and seasonal analysis.

$$\nabla x_t = x_t - x_{t-1} \quad (6)$$

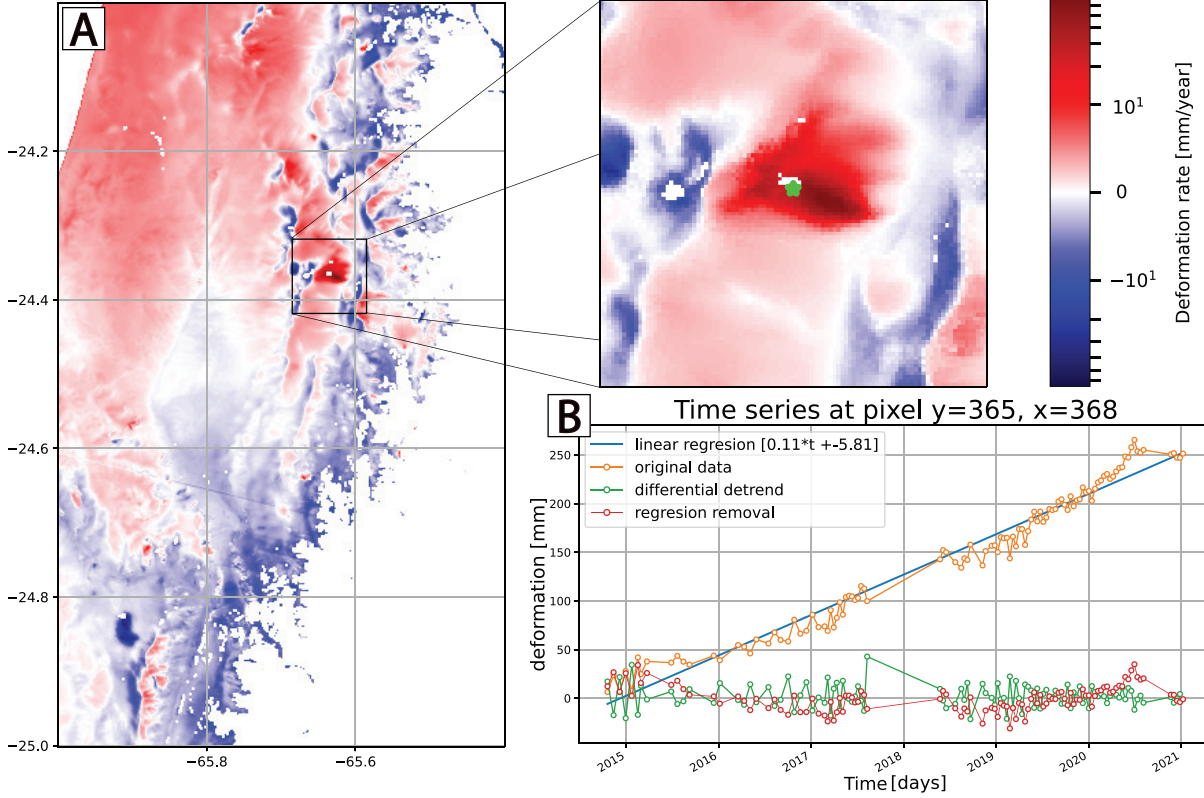


Figure 3: A) Regional calculated velocity map zoomed to the selected landslide. B) Time series of a single pixel with approaches for detrending the data. Note the better stability on the differential detrend.

The first approach consists in grouping up the detrended deformation values by year to observe if there are any repetitive variations between years. After this, the deformation values were separated into two samples, one that includes values during the rainy season (November-April) and the dry season (May-October). with these two samples, histograms were created to visualize the displacement values distribution. Also the comparison of the two empirical cumulative distributions ($H_1(x), H_2(x)$) using the Kolmogorov-Smirnov statistic (Equation 7) determine if two populations make part of the same distribution or not (Smirnov, 1939). The target statistic (D) was found by using the python *SciPy* package.

$$D = \sup |H_1(x) - H_2(x)| \quad (7)$$

4 Results

The resulting LOS velocity field shows movements relative to the satellite, for this reason most of the displacement on the mountain eastern flanks appear to be positive (towards the

satellite) and on the western flanks, they are moving away from the satellite. In the regional scale, the movement magnitudes range between 0 and ca. 60 mm/year for the fastest moving zones. The selected landslide sample is located in the $12m^2$ area surrounding the point 24.36°S, 65.63°W, it can be described as a fan shaped landslide with 4 lobes downslope. The LOS velocities for this landslide show a mean, median and standard deviation values of 21.82, 17.27 and 13.55 mm/year respectively. The same values after the downslope projections are 8.98, 6.99 and 6.42 mm/year respectively (Figure 4). In this report all velocities slower than 1 mm/year and negative velocities were excluded to avoid misinterpretations.

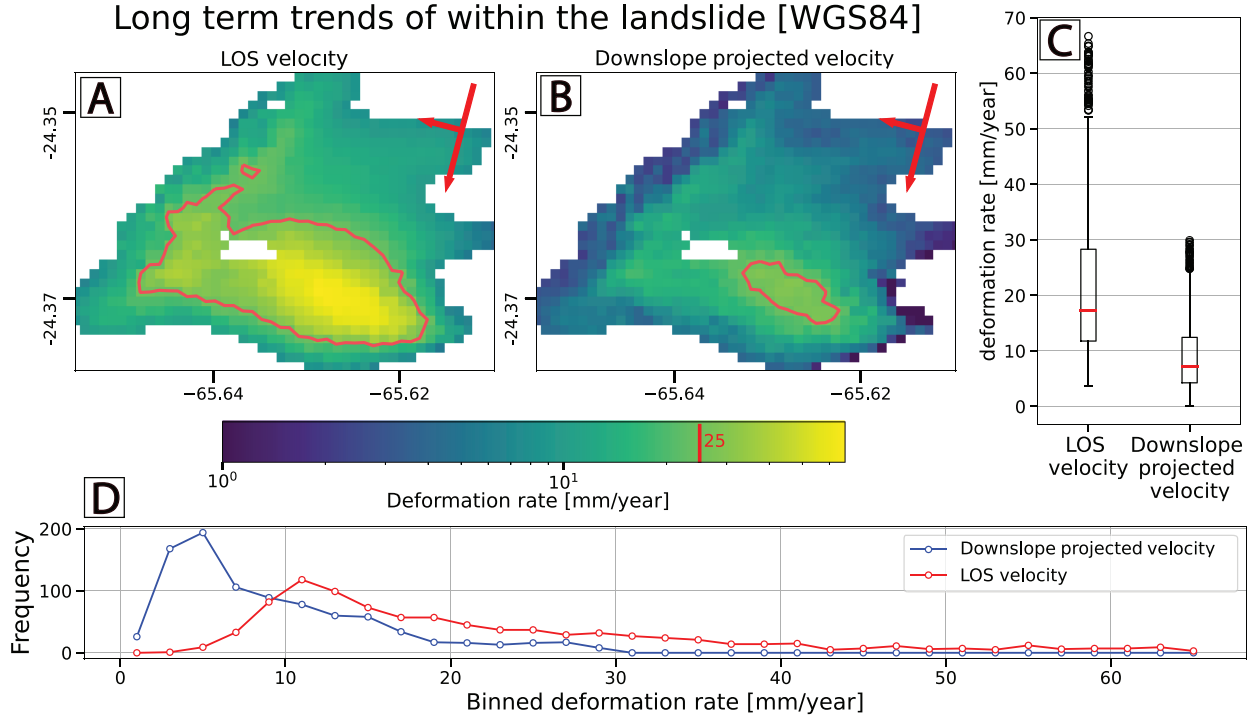


Figure 4: A) LOS and velocity field for the selected landslide. B) Downslope projected velocity field. On the maps the red contour surrounds the areas with velocities higher than 25mm/year. C) Velocity distributions box-plots. D) Velocities histograms.

To map unstable terrains and slow-moving landslides for the entire area, contours were drawn on the downslope projected velocity field on intervals of 5 mm/year. Without any kind of polygon manipulations, 251 polygons were drawn where terrain velocities are at least 10 mm/year. Also, 11 polygons were produced to describe areas with velocities higher than 25 mm/year. It is important to mention that these areas were found on both mountain flanks (Appendix).

Regarding the seasonal variation assessment, the yearly detrended deformation values for a single pixel in the selected landslide apparently cover a narrower range during the dry season (Ca. 15 mm) and during the humid season these values reach up to 22 mm (Figure 5). This is a simple observation, that leads to a better statistical analysis. By using all

the time series in the area, it was found that the distribution of the deformation during the dry season has a local mode between 6-8 mm, this mode is not present in the humid season distribution but there is another one between 17-19 mm (Figure 6). The Kolmogorov-Smirnov test displayed a D value equal to 0.85 and a probability p of 0, this suggests that the null hypothesis H_0 should be rejected, in other words, these are drawn from different distributions and humid/dry season have different velocity distributions.

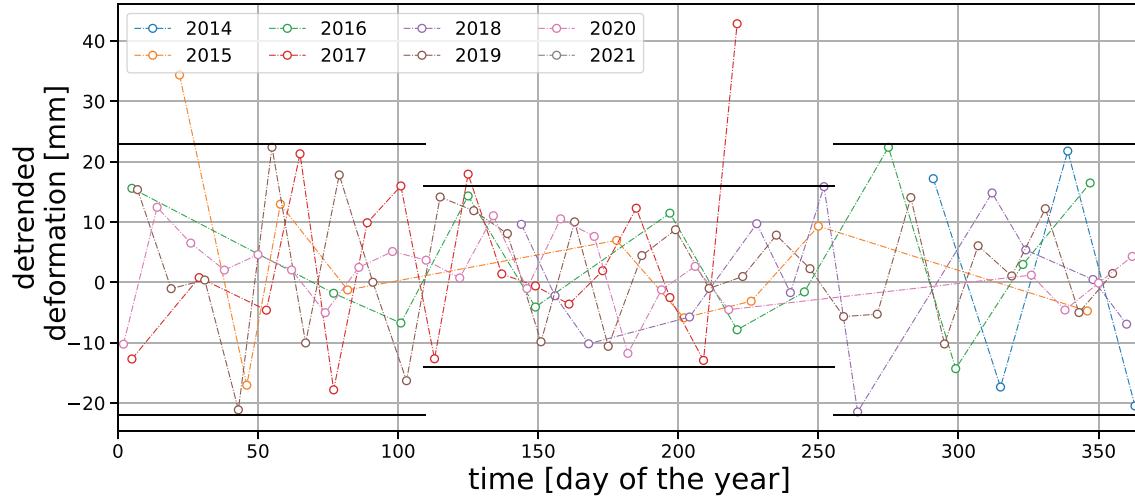


Figure 5: Detrended deformation values on a yearly scale, horizontal lines are subjective bounds excluding extreme values

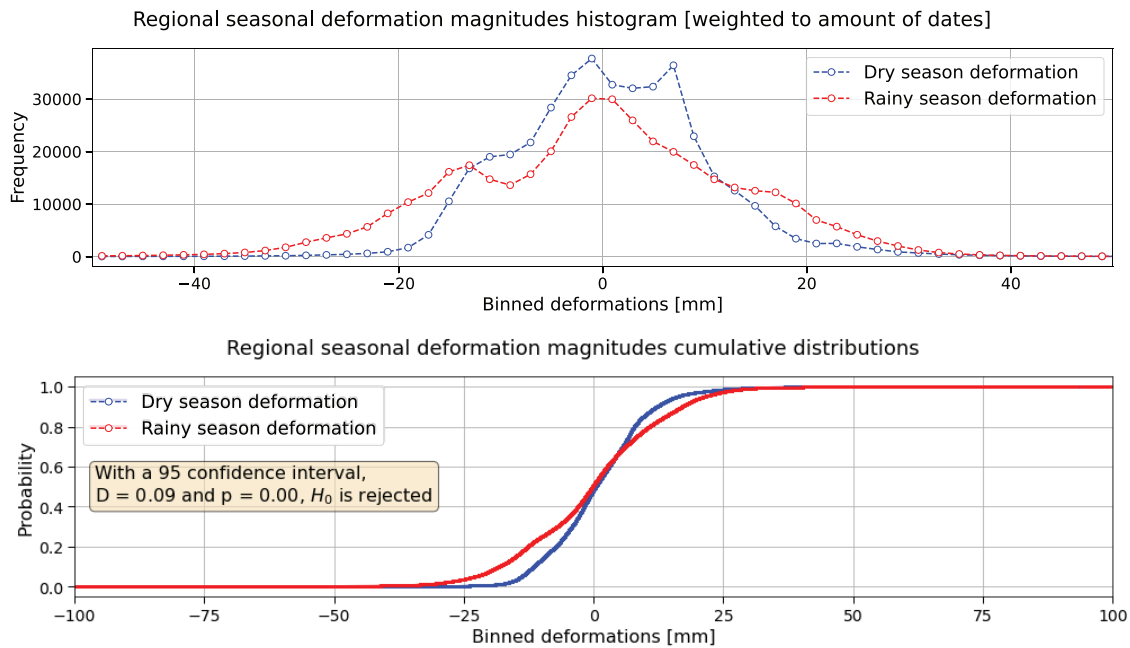


Figure 6: A) Detrended deformation histograms for the humid and dry seasons (extreme values are not shown) B) Cumulative distributions for both samples and the Kolmogorov-Smirnov test results

5 Discussion

5.1 LiCSBAS results and velocity fields

Overall the quality of the time series is not perfect because it has a few gaps and one lack of information during 2018, but it is still very good and allows to understand the general displacements. It's spatial resolution allowed to identify some movement areas with only one or two pixels. Thanks to the environment conditions of the area, the overall coherence is very well preserved in these high elevation mountains adding confidence on the displacement values. For the velocity field resulting from the downslope projection of LOS velocities, it was found that all landslides can be classified as extremely slow or very slow (WP/WLI, 1995; Cruden & Varnes, 1996; Hungr *et al.*, 2013). This approach appears to work well on mapping the velocity of hillslope processes. The mapping appears to work very well on east facing slopes due to the nature of descending track acquisition, still landslides were also detected on the opposite flank. Some negative velocities were reported on the west facing flanks, this suggests that terrain moves uphill, this is very unlikely. It is worth to investigated whether these velocities are the product of an artifact, noise in the data or if they reflect any other kind of deformation. Finally, slope values for the unstable terrains range between 12 and 36°, this is a good range of slopes to identify features.

5.2 Seasonal influence

It was found that there is a different distribution of velocities during the dry and wet seasons. These still do not show drastic changes in the velocity variations, which could lead to accept the first order polynomial fit on the deformation time series to describe the velocity model. Further analysis with other data sources is recommended to establish what is the real influence of variable rainfall on the regional or local scale.

6 Conclusions

Time series analysis is a very promising tool for slow moving landslide identification on large study areas, it appears to be a relatively fast and not computational demanding as well. In this study, the potential of LiCSBAS is shown for the mapping of unstable terrains associated to slow moving landslides. Even though the time series only covers from 2014 to 2020, SAR data is continuously being acquired, increasing the availability of data for better analysis. Usage of both, ascending and descending tracks is recommended when available to provide much better field velocities for both mountain faces.

The area of the Eastern cordillera and Subandean ranges contains abundant slow and extremely slow moving landslides, this is very important information for society, since it can prevent life and economical losses due to this persistent hazard. On the regional scale deformation values indicate that there is a slight influence of seasonality in the velocity fields, this is worth to be tested on smaller study areas, this way results can be better analyzed.

References

- [1] ESA Sentinel Data Access, <https://sentinel.esa.int/web/sentinel/sentinel-data-access>
- [2] Bianchi D, Yañez A. (1992). Las precipitaciones en el NOA Argentino. Segunda Edición. Salta: INTA.
- [3] Cascini, L., Fornaro, G., & Peduto, D. (2010). Advanced low-and full-resolution DInSAR map generation for slow-moving landslide analysis at different scales. *Engineering Geology*, 112(1-4), 29-42.
- [4] Cruden, D. M. (1993). Cruden, DM, Varnes, DJ, 1996, Landslide Types and Processes, Special Report, Transportation Research Board, National Academy of Sciences, 247: 36-75.
- [5] Garreaud RD, Aceituno P. (2007). Atmospheric circulation and climatic variability. In: Veblen T, Young R, Orme AR, editors. *The physical geography of South America*. Oxford: Oxford University Press; p. 45–59.
- [6] Esper Angillieri, M. Y., Perucca, L., & Vargas, N. (2020). Spatial and temporal analysis of debris flow occurrence in three adjacent basins of the western margin of Grande River: Quebrada de Humahuaca, Jujuy, Argentina. *Geografiska Annaler: Series A, Physical Geography*, 102(2), 83-103.
- [7] Hanssen, R. F. (2001), Radar Interferometry: Data Interpretation and Error Analysis, Heidelberg (978-0-7923-6945-5) Springer Verlag. <http://dx.doi.org/10.1007/0-306-47633-9>
- [8] Hungr, O., Leroueil, S., & Picarelli, L. (2014). The Varnes classification of landslide types, an update. *Landslides*, 11(2), 167-194.
- [9] International Geotechnical Society's UNESCO Working Party on World Landslide Inventory(WP/WLI. (1995). A suggested method for describing the rate of movement of a landslide. *Bulletin of the International Association of Engineering Geology*, 52, 75-78.
- [10] Iverson, R. M. (2000). Landslide triggering by rain infiltration. *Water resources research*, 36(7), 1897-1910.
- [11] May, J. H. (2008). A geomorphological map of the Quebrada de Purmamarca, Jujuy, NW Argentina. *Journal of Maps*, 4(1), 211-224.
- [12] Morishita, Y., Lazecky, M., Wright, T. J., Weiss, J. R., Elliott, J. R., & Hooper, A. (2020). LiCSBAS: An open-source InSAR time series analysis package integrated with the LiCSAR automated Sentinel-1 InSAR processor. *Remote Sensing*, 12(3), 424.
- [13] Lazecký, M., Spaans, K., González, P. J., Maghsoudi, Y., Morishita, Y., Albino, F., ... & Wright, T. J. (2020). LiCSAR: An automatic InSAR tool for measuring and monitoring tectonic and volcanic activity. *Remote Sensing*, 12(15), 2430.

- [14] (SEGEMAR) Argentina. Servicio Geológico Minero Argentino. Instituto de Geología y Recursos Minerales, Salfity, José A., Monaldi, César R., Guidi, F., Salas, R.J. (1998). Mapa Geológico de la Provincia de Salta. oai: <https://repositorio.segemar.gov.ar:308849217/1525>
- [15] (SEGEMAR) Argentina. Servicio Geológico Minero Argentino. Instituto de Geología y Recursos Minerales, Coira, B.L.L., Zappettini, E.O., Ferpozzi, F.J. (2008). Mapa Geológico de la Provincia de Jujuy. oai: <https://repositorio.segemar.gov.ar:308849217/1517>
- [16] Smirnov, N. V. (1939). On the estimation of the discrepancy between empirical curves of distribution for two independent samples. Bull. Math. Univ. Moscou, 2(2), 3-14.
- [17] Swanson, F. J., & Swanston, D. N. (1977). Complex mass-movement terrains in the western Cascade Range, Oregon. Reviews in Engineering Geology, 3, 113-124.
- [18] Weiss, J. R., Walters, R. J., Morishita, Y., Wright, T. J., Lazecky, M., Wang, H., ... & Parsons, B. (2020). High-resolution surface velocities and strain for Anatolia from Sentinel-1 InSAR and GNSS data. Geophysical Research Letters, 47(17), e2020GL087376.
- [19] Yu, C., Li, Z., Penna, N., & Crippa, P. (2018, April). Generic Atmospheric Correction Online Service for InSAR (GACOS). In EGU General Assembly Conference Abstracts (p. 11007).

7 Appendix

